Electronic Supporting Information (ESI)

Preparation of ultrathin Pt electrocatalyst *via* galvanic replacement reaction of electrodeposited CuCl for oxidation of methanol in alkaline medium

Long Chao,[a] Nian Liu,[a] Xiujuan Xiong,[a] Fang He,[a] Ting Huang,[a] Qingji Xie[a]* and Shouzhuo Yao[a,b]

[a]Key Laboratory of Chemical Biology and Traditional Chinese Medicine Research (MOE of China), National & Local Joint Engineering Laboratory for New Petro-chemical Materials and Fine Utilization of Resources, Hunan Normal University, Changsha 410081, China.

[b]State Key Laboratory of Chemo/Biosensing and Chemometrics, Hunan University, Changsha 410082, P.R. China.

*Correspondence should be addressed to Qingji Xie (xieqj@hunnu.edu.cn)

Contents

1. Experimental Section

1.1. Instrument and reagents

A CHI660A electrochemical workstation (CH Instrument Co.) and a conventional three-electrode electrolytic cell were used in all electrochemical experiments. The working electrode was a 3 mm diameter disk Au electrode, a 3 mm diameter disk Pt electrode, a 3 mm diameter disk glassy carbon electrode (GCE), or a quartz crystal microbalance (QCM) Au electrode (or one of their modified electrodes), the reference electrode was a KCl-saturated calomel electrode (SCE), and the counter electrode was a graphite rod. All potentials reported here are cited versus SCE. A computer-interfaced HP4395A impedance analyzer was employed in the QCM experiments. We employed AT-cut 9 MHz QCM Au electrodes (key-hole configuration, Model JA5, Beijing Chenjing Electronic Co., China). Scanning electron microscopy (SEM) characterizations with energy-dispersive X-ray spectroscopy (EDX) were collected on a JEM-6700F field emission scanning electron microscope. X-ray diffraction (XRD) patterns were collected on a D8 Discover X-ray diffractometer (Bruker Co., USA). X-ray photoelectron spectroscopy (XPS) characterizations were conducted on an XPS instrument (Thermo fisher scientific, UK) equipped with a monochromatic Al K*a* radiation (*E* = 1486.6 eV). Inductively coupled plasma atomic emission spectroscopy (ICP-AES, Baird, USA) was used to determine the mass load of Pt using its 265.9 nm spectrum line. To simulate the surface modifications for GCE here, the QCM Au electrodes before and after the same modifications were used for XPS and XRD characterizations.

$HAuCl_4 \cdot 4H_2O$, K_2PtCl_4 and $CuSO_4 \cdot 5H_2O$ were purchased from Chemicals Company of Tianjin (Tianjin, China). Methanol, KOH, HCl, H_2SO_4 and $K_4Fe(CN)_6 \cdot 3H_2O$ were purchased from Sinopharm Chemicals Co., Ltd. (Shanghai, China). All chemicals were of analytical grade or better quality, and all the solutions were prepared using Milli-Q ultrapure water (Millipore, >18 MΩ·cm).

1.2. Preparation and characterization of modified electrodes

At first, cleaning of the GCE was conducted as before.[1] Firstly, the GCE was mechanically polished with alumina powder to a mirror finish. After water-rinse, the polished GCE was ultrasonically treated sequentially in water, ethanol and water for 5 min each to remove residual alumina powder. The GCE was further treated by cyclic voltammetry (CV, −1.0~1.0 V, 50 mV s^{-1}) in 0.5 M aqueous H_2SO_4 until reproducible cyclic voltammograms were obtained. After water-rinse, the GCE was characterized by CV (0.1~0.5 V, 50 mV s^{-1}) in 0.2 M aqueous Na_2SO_4 containing 2.0 mM $K_4Fe(CN)_6$. The peak-to-peak separation of the $Fe(CN)_6^{3-/4-}$ redox peaks was below 75 mV, indicating that the GCE had been well cleaned.

The $Pt_{(CuCl)x}$/Au/GCE was fabricated as illustrated in Scheme 1 and described below, (1) Au was electrodeposited on GCE in 0.05 M aqueous H_2SO_4 containing 2 mM $HAuCl_4$ at −0.2 V for 150 s (Au/GCE) under stirring conditions; (2) after sufficient rinse with pure water, CuCl was electrodeposited on Au/GCE (CuCl/Au/GCE) at −0.07 V in 100 mM aqueous HCl containing 20 mM $CuSO_4$; (3) after quick rinse of CuCl/Au/GCE with ultrapure water, CuCl/Au/GCE was immersed in a N_2-saturated 1 mM K_2PtCl_4 + 0.05 M H_2SO_4 aqueous solution for 15 min, allowing the GRR to occur as completely as possible ($Pt_{(CuCl)1}$/Au/GCE). Repeating the above steps (2) and (3) can obtain ultrathin Pt on Au/GCE ($Pt_{(CuCl)x}$/Au/GCE, here *x* denotes the number of CuCl-electrodeposition/GRR cycles). The as-prepared $Pt_{(CuCl)x}$/Au/GCEs were rinsed with ultrapure water, and then subjected to CV (−0.3~1.45 V, 50 mV s^{-1}) treatment in 0.5 M aqueous H_2SO_4 until reproducible cyclic voltammograms appeared. Linear sweep anodic stripping voltammetry (LSASV) was used to estimate the mass of deposited CuCl. According to the previous reports,[2-4] the real surface area of Pt ($S_{r\text{-}Pt}$) is estimated from the hydrogen adsorption (H "UPD") charge by using a conversion factor of 210 μC cm^{-2}, and the real surface area of Au ($S_{r\text{-}Au}$) is estimated from charge of reduction peak for Au oxides by using a conversion factor of 390 μC cm^{-2} in 0.5 M aqueous H_2SO_4, respectively.

In our opinion, the UPD simply means the (sub)monolayer underpotential deposition of an UPD material on a specific substrate surface at an UPD potential, and the energy at the UPD potential is obviously lower than that at the bulk-deposition thermodynamic potential. The driving force for (sub)monolayer UPD is originated from the strong and intrinsic intermolecular/atomic interaction between the specific UPD material (not limited to metal) and the specific substrate material, since the driving force can compensate the energy difference between the bulk-deposition thermodynamic potential and the UPD potential. It is well known that the atomic hydrogen shows a strong affinity to atomic Pt, namely, (sub)monolayer deposition of atomic H is energetically facilitated by the strong interatomic H-Pt interaction, which makes the reduction of H^+ to form (sub)monolayer-deposited atomic hydrogen on atomic Pt (i.e., (sub)monolayer adsorption of atomic H) at a potential positive of the bulk reduction potential of H^+ to H_2. Therefore, the adsorption/desorption of (sub)monolayer atomic hydrogen on Pt surface is rather similar to the UPD/stripping of a metal in principle, as reported in many literatures.[2, 5, 6] However, the products of UPD and bulk deposition of a metal are both metal atoms, but the product of the bulk electroreduction of H^+ is molecular hydrogen rather atomic hydrogen (atomic hydrogen is the product of underpotential electroreduction of H^+). In this sense, we thus write hydrogen "UPD" ad-/desorption instead of hydrogen UPD ad-/desorption here to highlight the similar principle but the existing differences between metal UPD and hydrogen UPD.

For comparison, ultrathin Pt modified Au/GCE was also prepared by UPD Cu and GRR ($Pt_{(Cu\text{-}UPD)y}$/Au/GCE, *y* denotes the number of UPD/GRR cycles) as reported.[7-9] Firstly, a full monolayer of Cu UPD was formed on Au/GCE (Cu_{UPD}/Au/GCE) by holding the potential at −0.01 V for 500 s in aqueous 0.1 M H_2SO_4 + 5 mM $CuSO_4$. After quick rinse of Cu_{UPD}/Au/GCE with ultrapure water, Cu_{UPD}/Au/GCE was immersed in a N_2-saturated 1 mM K_2PtCl_4 + 0.05 M H_2SO_4 aqueous solution for 15 min, allowing the GRR of Cu UPD atoms to occur as completely as possible. Repeating the above procedures, $Pt_{(Cu\text{-}UPD)y}$/Au/GCEs were obtained.

The pulse-electroplated Pt modified Au/GCE (Pt_p/Au/GCE) was prepared in 1 mM K_2PtCl_4 + 0.05 M H_2SO_4 solution. Pulse potential: 0.75 to −0.2 V; pulse width: 0.25 s, and pulse time 3 s. The Pt mass of as-prepared Pt_p/Au/GCE and Pt/C/Au/GCE are approximately equal to that of $Pt_{(CuCl)1}$/Au/GCE (about 0.4 μg). Commercial Pt/C (20%) catalyst modified electrode was fabricated as follows. 0.5 mg Pt/C (20%) catalyst was ultrasonically dispersed into 1 mL ultrapure water, and 4 μL of the suspension was dropped on the surface of Au/GCE. After drying, 5 μL of 0.5 wt% Nafion alcohol solution was cast on the electrode surface, drying at room temperature before use (Pt/C/Au/GCE). For comparison, Pt/C/Au/GCE without modification of electron-insulating Nafion was also prepared simply without the above Nafion-coating step. Without the Nafion modification, the Pt/C is not very robustly attached to the electrode surface and can only be used for a very limited number of trials.

The mass load of Pt for relevant modified electrodes was also determined by the ICP-AES method, and the detailed procedures are given as follows. 30 μL of fresh prepared aqua regia (3:1, V_{HCl}/V_{HNO3}, highly corrosive, treat with great care) was cast on the modified GCE surface for 5 min to dissolve Pt and Au, and then the solution was carefully transferred into a tumbler. Repeating the noble-metal-dissolution process for 4 times can fully dissolve the Pt and Au. In order to reliably determine the mass load of Pt by ICP-AES, each lysate solution was collected from five parallel modified electrodes prepared under the same condition to achieve a higher Pt content in a diluted aqua regia and the total volume of diluted aqua regia was 5 mL. The obtained solution was fed into an ICP-AES instrument (Baird, USA) to determine the concentration of Pt by using a proper calibration curve. Thus, the mass load of Pt at a relevant modified electrode can be obtained as the product of the ICP-AES-revealed Pt concentration and the solution volume.

1.3. Electrocatalytic experiments

Electrocatalytic oxidation of methanol was carried out by CV in 0.5 M KOH + 1.0 M CH_3OH. Chronoamperometry tests were also investigated at −0.3 V by recording the current-

time (*i*-*t*) curves. All of the solutions were deoxygenated by bubbling high-purity N_2 for at least 10 min prior to each measurement.

Theoretical estimation of the mass of a compact CuCl monolayer (Scheme S1)

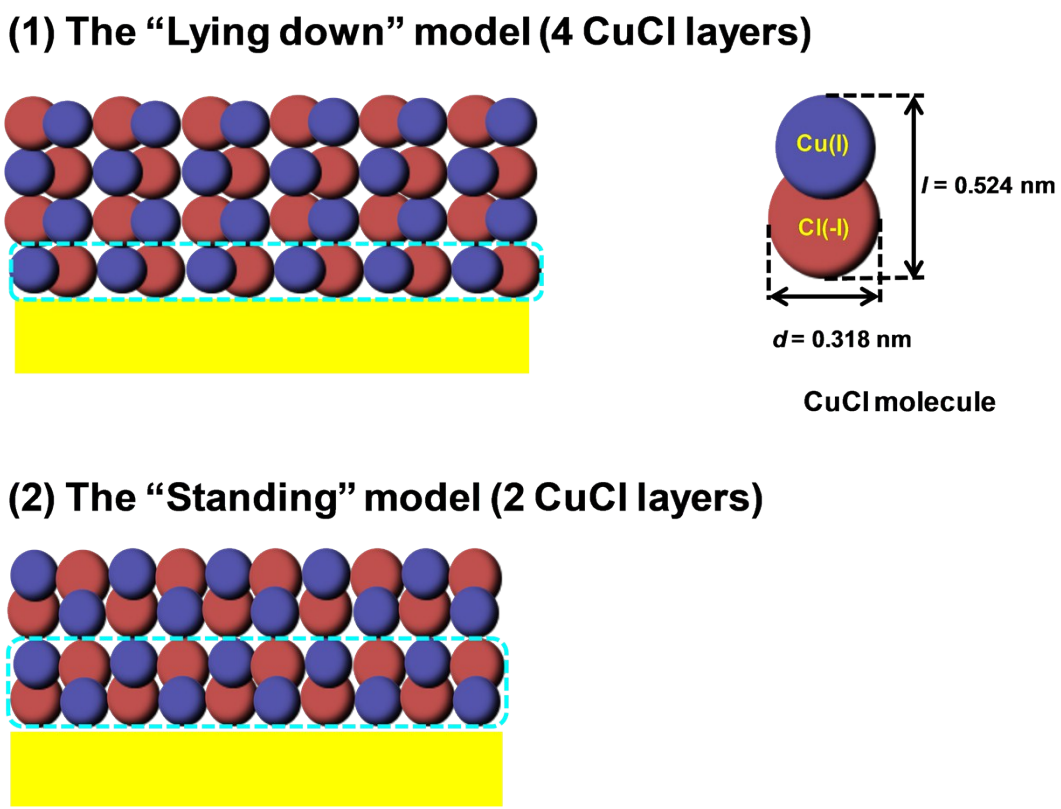

Scheme S1. Schematic illustration of the compact stacking of CuCl molecules on a flat electrode surface. Each dashed-rectangle-enclosed area indicates one CuCl monolayer.

In order to estimate the thickness of CuCl thin film, we theoretically examine the compact stacking of CuCl molecules on a flat electrode surface. The dimer structure of CuCl molecule (Cu_2Cl_2) may exist,[10] we thus consider the compact stacking of both CuCl and Cu_2Cl_2 molecules. The size of CuCl molecule can be calculated as about 0.524 nm × 0.318 nm based on the corresponding van der Waals atomic radii and covalence bond length.[11-13] We discuss two models, the "Lying down" model and the "Standing" model, for compact stacking of CuCl molecules, as shown in Scheme S1.

(1) The "Lying down" model. In this case of compact stacking of CuCl molecules, the number (N) and mass (m) of one compactly stacked CuCl monolayer per unit area (1×1 cm^2) can be estimated as follows.

$N = (1/d)\times(1/l) = (1/0.318\times10^{-7})\times(1/0.524\times10^{-7}) = 6.00\times10^{14}$ CuCl molecules cm^{-2}

$m = (N/N_A)\times M_{CuCl} = (6.00\times10^{14}/6.02\times10^{23})\times98.999 = 98.7$ ng cm^{-2}

where d is the bottom diameter of CuCl molecule, and l is its length.

In this case of compact stacking of Cu_2Cl_2 molecules, the number (N) and mass (m) of one compactly stacked CuCl monolayer per unit area (1×1 cm^2) can be estimated as follows.

$N = (1/2d)\times(1/l) = (1/2\times0.318\times10^{-7})\times(1/0.524\times10^{-7}) = 3.00\times10^{14}$ Cu_2Cl_2 molecules cm^{-2} = 6.00×10^{14} CuCl molecules cm^{-2}, so still $m = (N/N_A)\times M_{CuCl} = (6.00\times10^{14}/6.02\times10^{23})\times98.999 =$ 98.7 ng cm^{-2}

where $2d$ is the bottom size of Cu_2Cl_2 molecule, and l is its length.

(2) The "Standing" model. In this case of compact stacking of CuCl molecules, the number (N) and mass (m) of one compactly stacked CuCl monolayer per unit area (1 × 1 cm^2) can be estimated as follows.

$N = (1/d)\times(1/d) = (1/0.318\times10^{-7})\times(1/0.318\times10^{-7}) = 9.89\times10^{14}$ CuCl molecules cm^{-2}

$m = (N/N_A)\times M_{CuCl} = (9.89\times10^{14}/6.02\times10^{23})\times98.999 = 163$ ng cm^{-2}

In this case of compact stacking of Cu_2Cl_2 molecules, the number (N) and mass (m) of one compactly stacked CuCl monolayer per unit area (1×1 cm^2) can be estimated as follows.

$N = (1/2d)\times(1/d) = (1/2\times0.318\times10^{-7})\times(1/0.318\times10^{-7}) = 4.944\times10^{14}$ Cu_2Cl_2 molecules cm^{-2} = 9.89×10^{14} CuCl molecules cm^{-2}, so still $m = (N/N_A)\times M_{CuCl} = (9.89\times10^{14}/6.02\times10^{23})\times98.999 =$ 163 ng cm^{-2}

In practice, the compact stacking of CuCl molecules is generally random, so we average the two m values of the two models as (98.7+163)/2 = 131 ng cm^{-2}, namely, a compactly stacked CuCl monolayer weighs 131 ng cm^{-2} on average. Therefore, the mass of one electrodeposited CuCl monolayer is 131×0.4 = 52.4 ng on the QCM Au electrode ($S_{r\text{-}Au}$ = 0.4 cm^2) and is 131×0.81 = 106 ng on the Au/GCE ($S_{r\text{-}Au}$ = 0.81 cm^2).

Theoretical estimation of the mass of a compact Pt monolayer (Scheme S2)

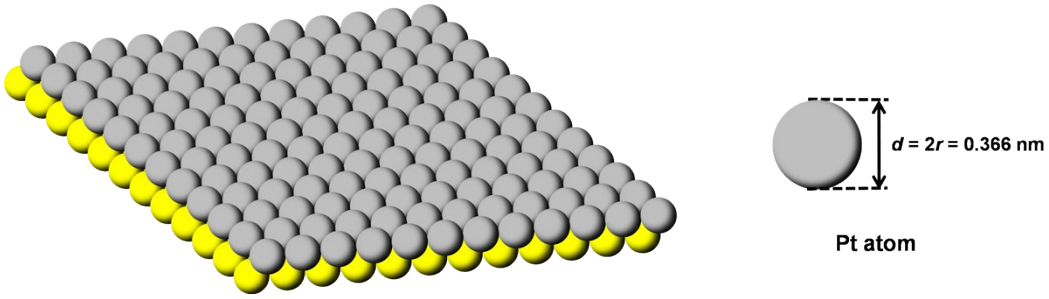

Scheme S2. Schematic illustration of the compact stacking of one atomic Pt monolayer on a flat Au surface.

We theoretically examine the compact stacking of one atomic Pt monolayer on a flat Au electrode surface, as shown in Scheme S2. According to the atomic radius of Pt (r = 0.183 nm, d=2r=0.366 nm), the number (N) and mass (m) of one monolayer Pt atoms per unit area (1×1 cm^2) can be estimated as follows.

$N = (1/d)\times(1/d) = (1/0.366\times10^{-7})\times(1/0.366\times10^{-7}) = 7.465\times10^{14}$ Pt atoms cm^{-2}

$m = N/N_A\times M(\mathrm{Pt}) = (7.465\times10^{14}/6.02\times10^{23})\times195.1 = 242$ ng cm^{-2}

Hence, the mass load of one atomic Pt monolayer on Au/GCE ($S_{r\text{-}Au}$ = 0.81 cm^2) is 242×0.81 = 196 ng.

Discussion on the thermodynamic possibility of GRR

The standard electrode potentials ($E^{\ominus}$, vs SHE) for the electrode reactions of CuCl/Cu and $PtCl_4^{2-}$/Pt are shown in Eqs. S1 and S2 below.

$$Cu^{2+} + Cl^- + e^- \rightarrow CuCl\ (s) \qquad E^{\ominus} = 0.538\ V \qquad (S1)$$

$$PtCl_4^{2-} + 2e^- \rightarrow Pt + 4Cl^- \qquad E^{\ominus} = 0.73\ V \qquad (S2)$$

The $E^{\ominus}$ difference as large as 0.192 V assures that the redox reaction (Eq. S3) is thermodynamically possible.

$$PtCl_4^{2-} + 2CuCl\ (s) \rightarrow Pt + 2Cu^{2+} + 6Cl^- \qquad (S3)$$

Discussion on the stoichiometry of the GRR processes

Here, the replacement efficiency (η) is defined as the molar ratio of replacement-deposited Pt atoms to electrodeposited Cu-UPD atoms or CuCl molecules, on the basis of the stoichiometry of the GRR processes.

1) **Estimation of η for Cu-UPD/GRR**. If the oxidation state of Cu is 0 (fully discharged during UPD of Cu from reduction of Cu^{2+}, two-electron transfer for Cu species), the expected GRR should be $PtCl_4^{2-} + Cu(0) \rightarrow Pt(0) + Cu^{2+} + 4Cl^-$, namely, the molar ratio of UPD Cu(0) to Pt(0) is 1:1, thus theoretically η=1. If the oxidation state of Cu is 0.5 (partially discharged during UPD of Cu from reduction of Cu^{2+}, 1.5-electron transfer for Cu species), the expected GRR should be $3PtCl_4^{2-} + 4Cu(0.5) \rightarrow 3Pt(0) + 4Cu^{2+} + 12Cl^-$, namely, the molar ratio of UPD Cu(0.5) to Pt(0) is 4:3, thus theoretically η=3/4=0.75. Obviously, the theoretical average of η is (1+0.75)/2=0.875 (average number of electrons transferred is n=(1+1.5)/2=1.75). Experimentally, a monolayer of Cu UPD on Au/GCE is 1.12 nmol UPD-Cu, as estimated from the electrical charge (1.89×10^{-4} C) for anodic stripping of Cu UPD in Fig. S5A (Q/nF=1.89×10^{-4}/(1.75×96485.3) =1.12 nmol). The 1.12 nmol UPD-Cu experimentally resulted in a Pt load of 0.142 μg (0.728 nmol Pt, Table S1 for y=1, $Pt_{(Cu\text{-}UPD)1}$/Au/GCE). Hence, the experimental η=0.728/1.12=0.65.

2) **Estimation of η for CuCl-electrodeposition/GRR**. The GRR should be $PtCl_4^{2-} + 2CuCl \rightarrow Pt + 2Cu^{2+} + 6Cl^-$ (two-electron transfer), namely, the molar ratio of CuCl to Pt(0) is 1:2, thus the theoretical η is 1/2=0.5. Experimentally, the electrodeposited CuCl (8.84 CuCl layers) on Au/GCE is 9.46 nmol CuCl, as calculated from the electrical charge (9.13×10^{-4} C) for anodic stripping of CuCl in Fig. S5A (Q/nF=9.13×10^{-4}/(1×96485.3)=9.46 nmol). The 9.46 nmol CuCl experimentally resulted in a Pt load of 0.4 μg (2.05 nmol Pt, Table S1 for x=1, $Pt_{(CuCl)1}$/Au/GCE). Hence, the experimental η=2.05/9.46=0.217.

As discussed above, both the theoretical and experimental η values of CuCl-electrodeposition/GRR do not improve when compared with those of Cu-UPD/GRR. However, our method can intrinsically provide more precursors (ultrathin and uniform multilayer CuCl) for GRR to obtain a thicker Pt deposit than conventional Cu-UPD/GRR method in one GRR cycle. The mass load and the equivalent number of compactly stacked atomic Pt monolayer on $Pt_{(CuCl)x}$/Au/GCE are nearly threefold those of $Pt_{(Cu\text{-}UPD)y}$/Au/GCE when $x = y$, respectively (Table S1). Hence, our method offers the advantage of more conveniently preparing a thicker Pt deposit than the conventional UPD/GRR method (Table S1, ESI†) in one single run, regardless of the higher replacement efficiency (both theoretical and experimental) of the conventional UPD/GRR method.

As shown in Figs. 3 and S12, the anodic peak current, the Pt-mass specific electrocatalytic activity ($SECA_m$) and the $S_{r\text{-}Pt}$-specific electrocatalytic activity ($SECA_a$) on $Pt_{(CuCl)1}$/Au/GCE at the peak potential (−0.05 V) are 9.5 mA, 23.7 mA μg_{Pt}^{-1} and 23 mA cm_{Pt}^{-2}, respectively; and the anodic peak current, the $SECA_m$ and the $SECA_a$ on $Pt_{(Cu\text{-}UPD)1}$/Au/GCE at the peak potential (0 V) are 2.03 mA, 14.7 mA μg_{Pt}^{-1} and 13.4 mA cm_{Pt}^{-2}, respectively. The electrocatalytic response of $Pt_{(CuCl)1}$/Au/GCE is notably higher than that of $Pt_{(Cu\text{-}UPD)1}$/Au/GCE. The different $SECA_m$ and $SECA_a$ on $Pt_{(CuCl)1}$/Au/GCE versus on $Pt_{(Cu\text{-}UPD)1}$/Au/GCE demonstrate that the catalytic performance of Pt in both cases is different. In practice, our method offers the advantage of more conveniently preparing a thicker Pt deposit than the conventional UPD/GRR approach. In our opinion, the catalytic performance of ultrathin Pt is affected by a combination of the surface area, the nano effects of Pt (size, morphology, and so on), and the substrate effect (Fig. S14), and to make clear the complicated mechanism (e.g. nano effects) requires more intensive researches in the future.

Table S1. The mass load of Pt estimated by ICP-AES, $S_{r\text{-}Pt}$, SSA_m and the equivalent number of compactly stacked atomic Pt monolayers for $Pt_{(CuCl)x}$/Au/GCEs and $Pt_{(Cu\text{-}UPD)y}$/Au/GCEs*

	x or *y*	1	2	3	4	5
$Pt_{(CuCl)x}$/Au/GCE	Pt load (μg)	0.400	0.828	1.28	1.76	-
	$S_{r\text{-}Pt}$ (cm^2)	0.417	0.567	0.697	0.752	
	SSA_m[a] (cm^2 μg^{-1})	1.04	0.685	0.545	0.427	-
	Equivalent number of compactly stacked atomic Pt monolayers	2.04	4.37	6.53	8.98	-
$Pt_{(Cu\text{-}UPD)y}$/Au/GCE	Pt load (μg)	0.142	0.281	0.410	0.575	0.690
	$S_{r\text{-}Pt}$ (cm^2)	0.150	0.288	0.426	0.488	0.552
	SSA_m[a] (cm^2 μg^{-1})	1.06	1.03	1.04	0.848	0.800
	Equivalent number of compactly stacked atomic Pt monolayers	0.720	1.43	2.10	2.93	3.52

* *x* denotes the number of the CuCl-electrodeposition/GRR cycles and *y* denotes the number of UPD/GRR cycles. [a] SSA_m is calculated from the ratio of $S_{r\text{-}Pt}$ in Fig. 1 to the Pt load. Here, with the increases of *x* and *y*, the SSA_m values of both electrodes are decreased. The specific surface area per Pt mass (SSA_m, listed in Table S1) of $Pt_{(CuCl)1}$/Au/GCE (1.04 cm^2 μg^{-1}) here is similar to that of $Pt_{(Cu\text{-}UPD)1}$ Au/GCE (1.06 cm^2 μg^{-1}). Obviously, the electrodeposited ultrathin multilayer CuCl is thicker than atomic (sub)monolayer Cu-UPD, and the equivalent number of compactly stacked atomic Pt monolayers is 2.04 (Table S1), versus 0.72 in the Cu-UPD case. The equivalent number of compactly stacked atomic Pt monolayers is introduced here to highlight that our method offers the advantage of more conveniently preparing a thicker Pt deposit than the conventional UPD/GRR method. Considering the better coverage of the Au substrate (Fig.1), it can be concluded that the first inner layer (more continuous than that in the UPD case) is succeeded by a more porous outer layer (i.e., the second layer). In fact, it is difficult to ideally form the continuous and compactly stacked Pt atomic layers for

$Pt_{(CuCl)1}$/Au/GCE, and very small Pt atomic clusters with a high SSA_m would be formed, due to possible aggregation of Pt atoms on the electrode surface in the GRR process. Anyway, our method possesses a higher preparation efficiency (conveniently preparing a thicker Pt deposit) of ultrathin Pt electrocatalyst simply in one single GRR cycle than that of Cu-UPD/GRR.

Table S2. Performance of typical Pt-based electrocatalysts toward methanol electrooxidation by CV in alkaline medium

Electrocatalyst[a]	Potential range of CV (V)	Scan rate ($mV\ s^{-1}$)	Conc. of methanol (M)	$SECA_m$[b] (mA μg_{Pt}^{-1})	Reference
p-Pt_1Cu_1/AP-GNPs	–0.8 to 0.6 vs SCE	50	0.5	3.61	[14]
Au/PtCu nanowires	–0.8 to 0.4 vs Ag/AgCl	50	1	1.5	[15]
rGO-Au@Pt NPs	–1.0 to 0.6 vs Ag/AgCl	50	0.5	6.245	[9]
Porous Pt NTs	–0.8 to 0.4 vs Ag/AgCl	50	1	2.84	[16]
Pt/Ag hollow Popcorns	–0.8 to 0.1 vs SCE	50	1	1.65	[17]
Pt/PANI/Pt	–0.7 to 0.2 vs SCE	20	1	2.2	[18]
Pt/$Ni(OH)_2$/rGO-4	–0.95 to 0.2 vs SCE	50	1	1.23	[19]
$Pt_{24}Pd_{26}Au_{50}$/Ppy	–0.8 to 0.8 vs Ag/AgCl	20	1	12.5	[20]
$Pt_{(Cu\text{-}UPD)1}$/Au/GCE	–0.7 to 0.2 vs SCE	50	1	14.7	This work
$Pt_{(Cu\text{-}UPD)3}$/Au/GCE	–0.7 to 0.2 vs SCE	50	1	9.75	This work
$Pt_{(CuCl)1}$/Au/GCE	–0.7 to 0.2 vs SCE	50	1	23.7	This work

[a] *p*-Pt_1Cu_1/AP-GNPs: uniform porous Pt-Cu nanocrystals supported on 1-aminopyrene functionalized graphene nanoplates; rGO-Au@Pt NPs: a thin layer of platinum on gold as Au@Pt core-shell nanoparticles on the surface of reduced graphene oxide; $Pt_{3.5}Pb$ NNWs: ultrathin $Pt_{3.5}Pd$ nerve-like nanowires; Pt/PANI: Pt modified polyaniline film on Pt. Pt/$Ni(OH)_2$/rGO-4: reduced graphene oxide modified with Pt nanocrystals and $Ni(OH)_2$ nanoparticles hybrid electrocatalysts; Ppy: polypyrrole. [b]

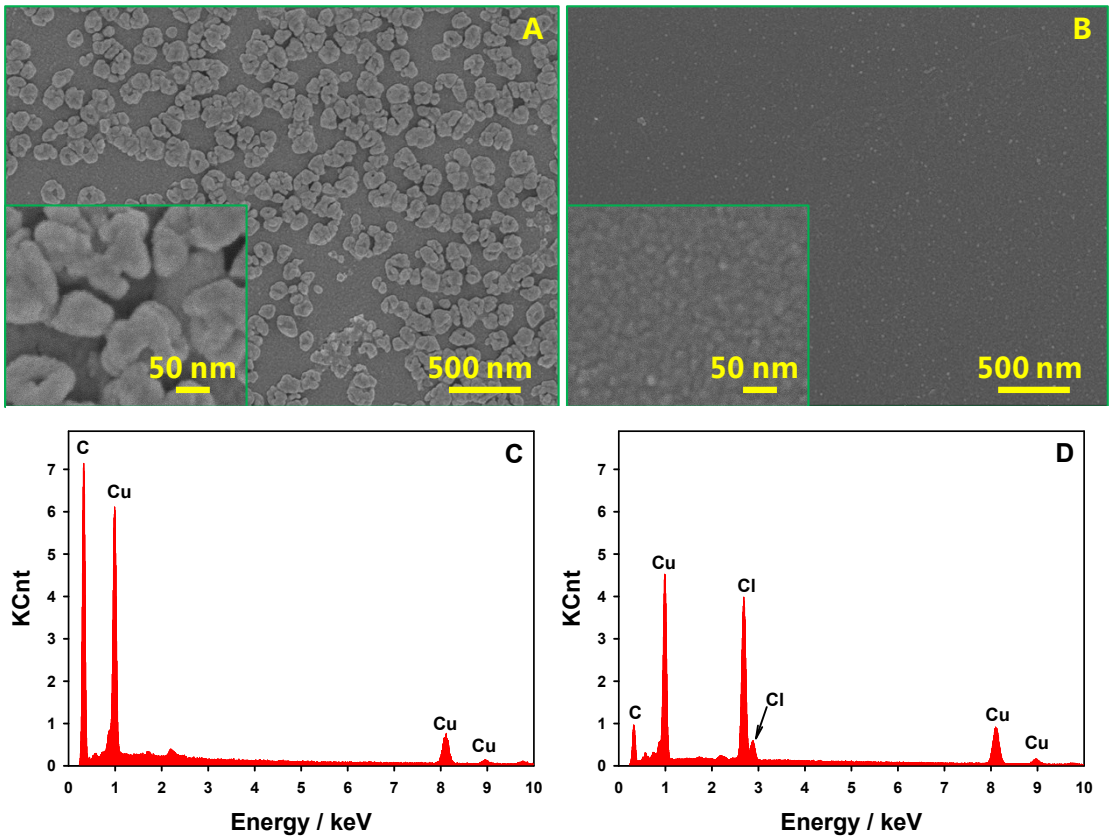

Fig. S1. SEM images and EDX results of Cu/GCE (A and C) and CuCl/GCE (B and D). Here, Cu was electrodeposited on GCE in 50 mM aqueous H_2SO_4 containing 20 mM $CuSO_4$ at −0.2 V for 100 s (Cu/GCE), and CuCl thin film was electrodeposited on GCE in 100 mM aqueous HCl containing 20 mM $CuSO_4$ at −0.07 V for 100 s (CuCl/GCE). Many small particles or small "islands" are seen on Cu/GCE (A), and the corresponding EDX results confirms the presence of abundant Cu element (C). In contrast, a rather uniform thin film is seen on CuCl/GCE (B), and the corresponding EDX results confirms the presence of Cu and Cl element (D). The results here have validated the principle depicted in Scheme 1(a).

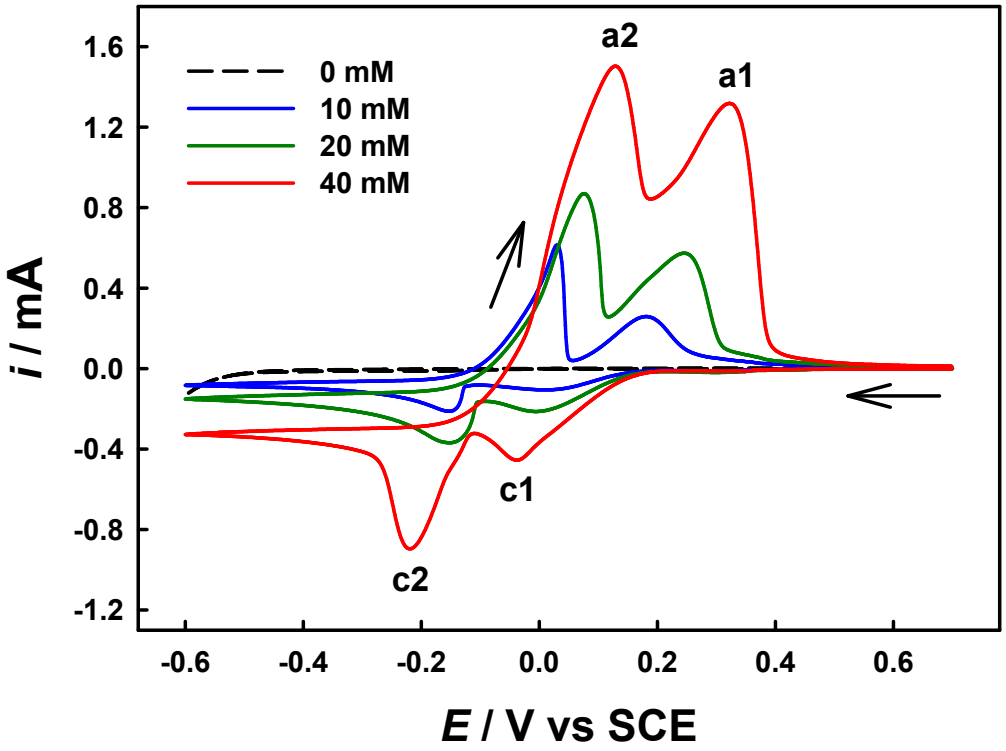

Fig. S2. CV curves on Au electrode in 100 mM aqueous HCl containing $CuSO_4$ at different concentrations (0, 10, 20 and 40 mM). Scan rate: 50 mV s^{-1}. Here, cyclic voltammetry (CV) at Au electrode in $CuSO_4$-free 100 mM HCl shows no redox peaks. In 10 mM $CuSO_4$ + 100 mM HCl, the cathodic peaks P_{c1} and P_{c2}, roughly at ca. 0.01 V and −0.15 V, are ascribed to electroreduction of Cu^{2+} to CuCl and then to Cu, respectively[21,22]. The corresponding anodic peaks at ca. 0.03 V and 0.18 V (P_{a2} and P_{a1}) represent oxidation of Cu(0) to CuCl and then to Cu^{2+}, respectively. As expected, each peak current increases and each peak potential normally shifts with the increase of Cu^{2+} concentration. After the negative potential limit is positively moved to −0.07 V, the redox peaks for UPD of Cu appears near ca. 0.3 V,[7, 8, 23] as discussed in Fig. S3.

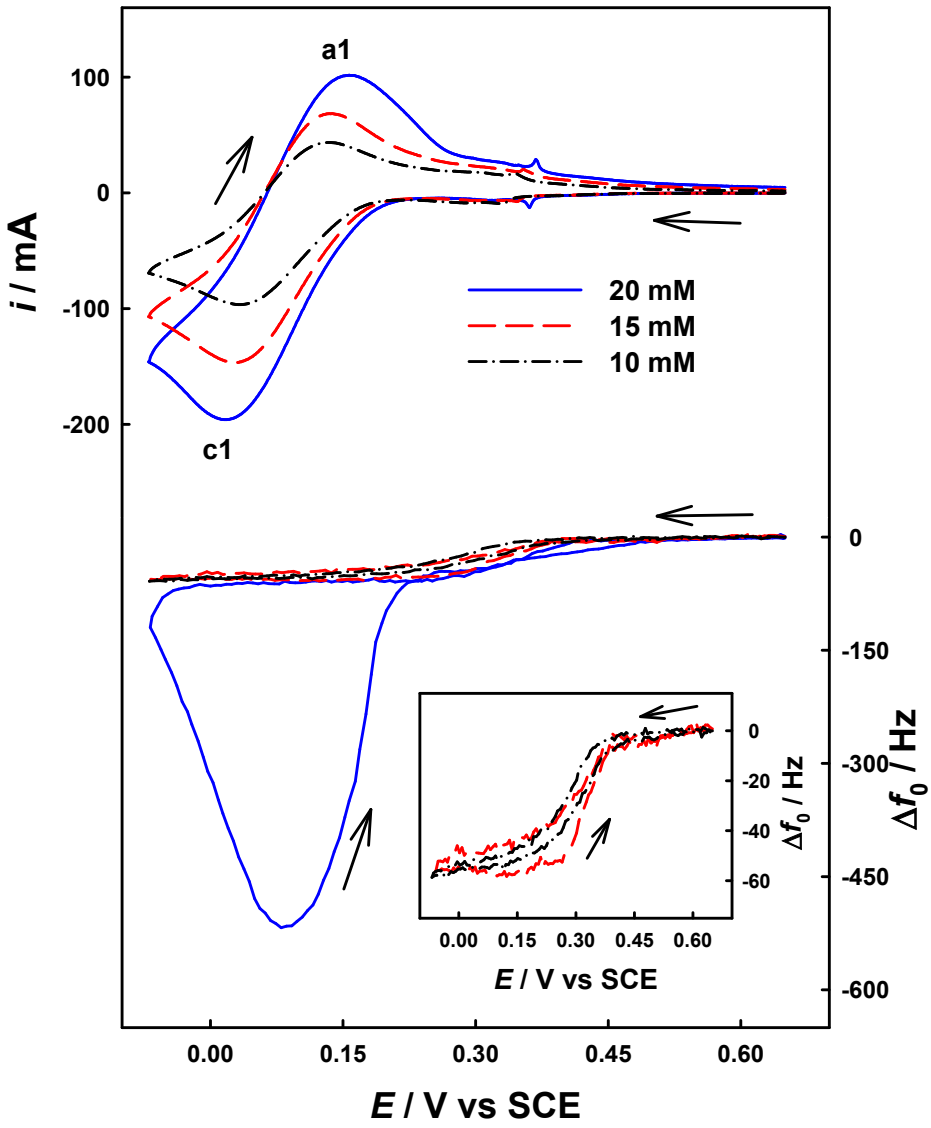

Fig. S3. Simultaneous responses of current and frequency changes (Δf_0) on bare QCM Au electrode during potential cycling with a negative potential limit of −0.07 V in 100 mM aqueous HCl containing $CuSO_4$ at different concentrations (10, 15 and 20 mM). Scan rate: 10 mV s^{-1}. Inset: Enlargement of Δf_0 obtained in 100 mM aqueous HCl containing 10 or 20 mM $CuSO_4$. We solely see frequency decrease/increase (Δf_0, ca. −/+55 Hz) resulting from the UPD/stripping of Cu in 100 mM aqueous HCl containing 10 mM or 15 mM $CuSO_4$ (ca. 42 ng of UPD Cu). The large frequency response to CuCl precipitation/stripping is seen in 100 mM aqueous HCl containing 20 mM $CuSO_4$, and the frequency decrease occurs notably behind the

cathodic peak of Cu^{2+}-to-CuCl reduction (P_{c1}), probably as a result of oversaturation of CuCl precipitation. The solubility product constant of CuCl is $K_{sp} = c(Cl^-) \times c(Cu^+) = 1.2\times10^{-6}$ and $c(Cl^-)$ is 100 mM here, so the calculated minimum concentration of Cu^+ for CuCl precipitation is $1.2\times10^{-6}/c(Cl^-) = 0.012$ mM. However, CuCl can also form soluble complexes with Cl^-,[24] and here we observed that $c(Cu^{2+})$ should be larger than 15 mM for precipitation of CuCl in 100 mM HCl. Thus, we selected 20 mM $CuSO_4$ for electrodeposition of CuCl.

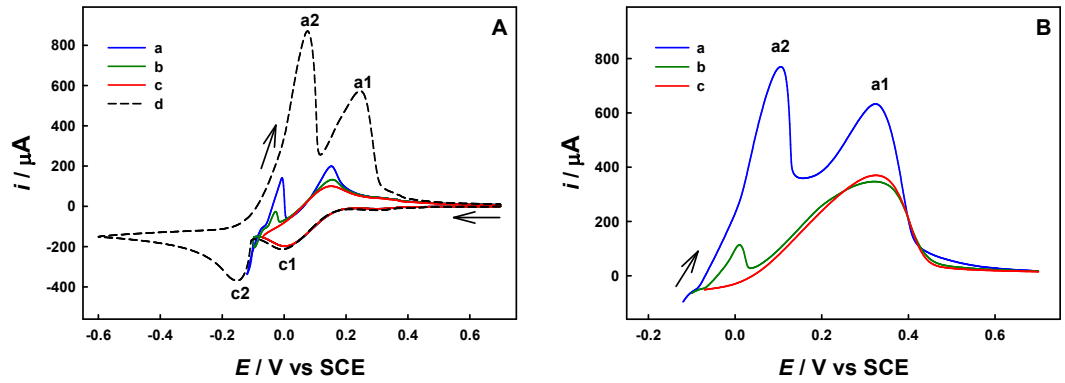

Fig. S4. (A) CV curves with different negative potential limits (a: –0.12 V, b: –0.1 V, c: –0.07 V and d: –0.6 V) and (B) LSASV curves on Au electrode after 30 s preconcentration at –0.12 V (a), –0.1 V (b) and –0.07 V (c). Solution: 20 mM $CuSO_4$ + 100 mM HCl. Scan rate: 50 mV s^{-1}. The CV experiments show that both the oxidation peaks of Cu(0) to CuCl and of CuCl to Cu^{2+} (P_{a2} and P_{a1}) appear for a negative potential limit at −0.6 V, or −0.12 V or −0.1 V (A). However, at a negative potential limit of −0.07 V, the oxidation peak of Cu(0) to CuCl (P_{a2}) disappears and only the oxidation peak of CuCl to Cu^{2+} (P_{a1}) is seen. The reduction peaks P_{c2} and P_{c1} change similarly with the shifting of negative potential limit. The LSASV curves after preconcentration for 30 s show that peaks P_{a2} and P_{a1} appear when the preconcentration potential is at −0.12 V or −0.1 V, but peak P_{a2} disappears and peak P_{a1} remains after preconcentration at −0.07 V (B). Both CV and LSASV experiments indicate that here only electrodeposition of CuCl but no bulk electrodeposition of Cu(0) occur at −0.07 V.

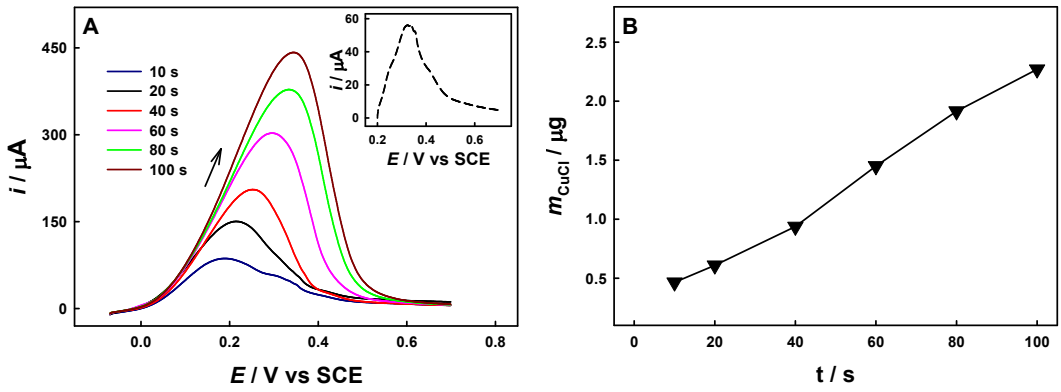

Fig. S5. (A) LSASV curves at –0.07 V in 100 mM HCl on CuCl/Au/GCEs that were obtained after potentiostating for different time at –0.07 V in 20 mM $CuSO_4$ + 100 mM HCl and then immediately rinsing with pure water. Inset: an independent LSASV experiment on Cu_{UPD}/Au/GCE that was obtained after potentiostating for 40 s at 0.2 V in 20 mM $CuSO_4$ + 100 mM HCl. (B) The corresponding mass of CuCl estimated from the electrical charge under the ASV peak on Au/GCE in 100 mM HCl. Here, after correcting the electrical charge for anodic stripping of Cu UPD (Inset of panel A) of ca. 1.89×10^{-4} C, the thickness of CuCl thin film obtained after 40 s preconcentration on Au/GCE ($S_{r\text{-}Au}$ = 0.81 cm^2) is calculated to be 0.937/0.106 = 8.84 CuCl layers according to Scheme S1.

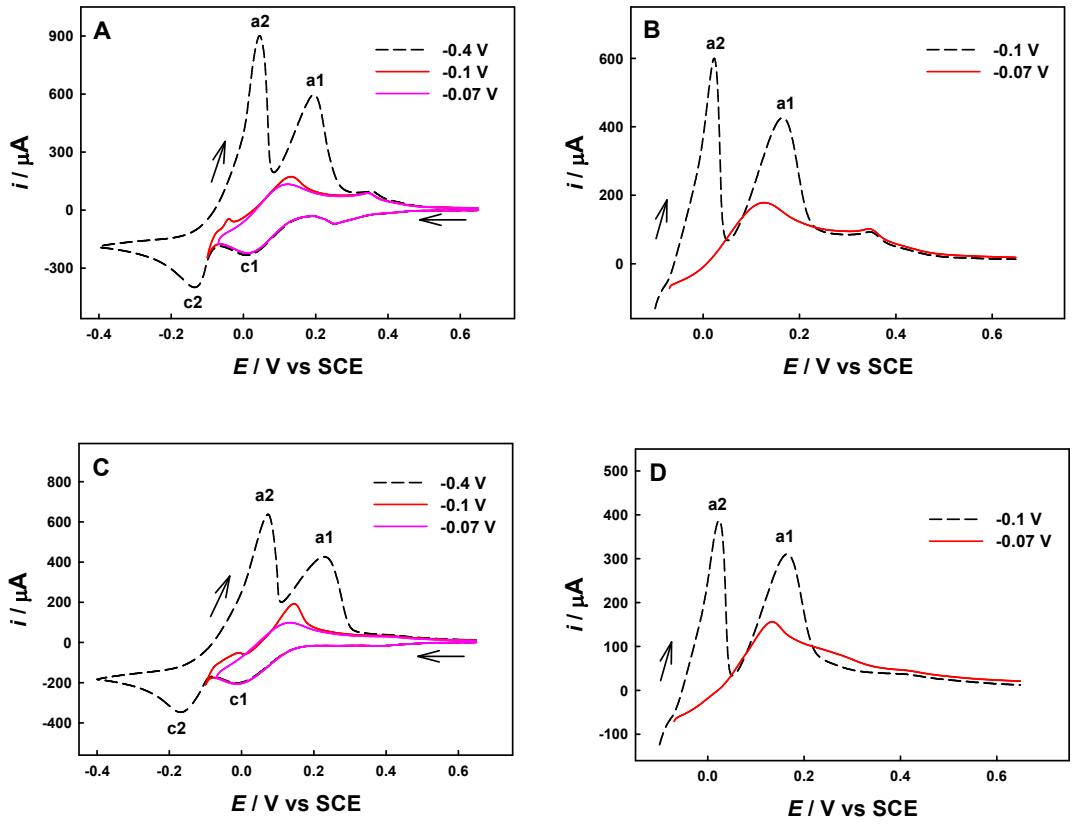

Fig. S6. CV curves of different negative potential limits (A) and LSASV curves after 30 s preconcentration at different potentials (B) on $Pt_{(CuCl)2}$/Au/GCE, as well as CV curves of different negative potential limits (C) and LSASV curves after 30 s preconcentration at different potentials (D) on commercially available bare Pt disk electrode. Solution: 20 mM $CuSO_4$ + 100 mM HCl. Scan rate: 50 mV s^{-1}. The CV experiments show that the oxidation peaks of Cu(0) to CuCl and of CuCl to Cu^{2+} (P_{a2} and P_{a1}) appear for a negative potential limit at −0.1 V or −0.4 V on $Pt_{(CuCl)2}$/Au/GCE (A). However, at a negative potential limit of −0.07 V, the oxidation peak of Cu(0) to CuCl (P_{a2}) disappears and only the oxidation peak of CuCl to Cu^{2+} (P_{a1}) is seen. The reduction peaks P_{c2} and P_{c1} change similarly with the shifting of negative potential limit. The LSASV curves after preconcentration for 30 s also show that peaks P_{a2} and P_{a1} appear when the preconcentration potential is at −0.1 V, but peak P_{a2} disappears and peak P_{a1} remains after preconcentration at −0.07 V (B). Both CV and LSASV experiments indicate that here only electrodeposition of CuCl but no bulk electrodeposition of Cu(0) occur at −0.07 V.

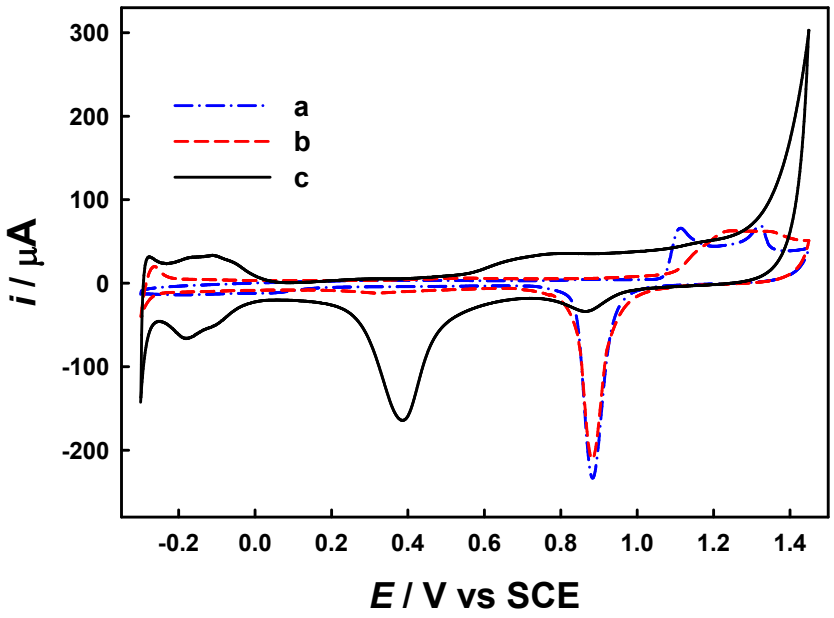

Fig. S7. CV curves of Au/GCE (a), and after immersion of Au/GCE in 1 mM K_2PtCl_4 for 15 min and then sufficient water rinse (b) and $Pt_{(CuCl)1}$/Au/GCE (c) in 0.5 M aqueous H_2SO_4. Scan rate: 50 mV s^{-1}. Here, $P_{c\text{-}Au}$ current is slightly decreased versus that of the original Au/GCE and a small current for hydrogen adsorption newly appears from −0.25 V to −0.3 V, and a weak reduction current of Pt oxides and solution-state O_2 appears at ca. 0.37 V, indicating that the Pt load here is negligibly small versus that of $Pt_{(CuCl)1}$/Au/GCE. The small Pt load results most likely from electroreduction of the small-quantity $PtCl_4^{2-}$ adsorbed on a rough Au surface,[25] which is not easy to be rinsed completely. In general, the Au/GCE gives no Pt signals, K_2PtCl_4-treated Au/GCE gives negligibly small signals of Pt, but $Pt_{(CuCl)1}$/Au/GCE gives much higher signals of Pt.

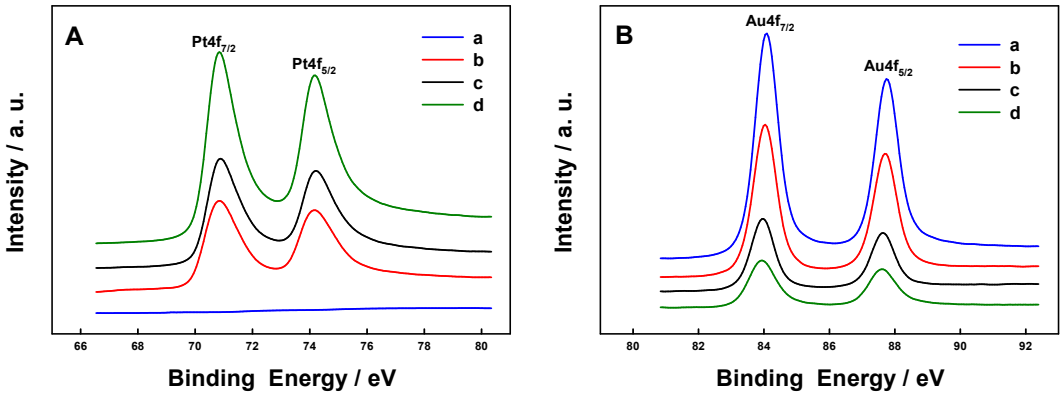

Fig. S8. XPS spectra of Pt4f (A) and Au4f (B) peaks for QCM Au (a), $Pt_{(CuCl)1}$/QCM Au (b), $Pt_{(CuCl)2}$/QCM Au (c) and $Pt_{(CuCl)4}$/QCM Au (d). Here, no Pt signals are seen on QCM Au, and the Pt signals are increased with the increase of *x* (*x*=1, 2, and 4 here). As expected, Pt signals are not seen on bare QCM Au. The $4f_{7/2}$ and $4f_{5/2}$ signals for Au appear at 84 and 87.7 eV, as well as those for Pt appear at 71 and 74.2 eV. The 4f signals for Pt are enhanced with the increase of *x*, but those for Au are weakened. The Au signals are the strongest on QCM Au, and the Au signals are decreased with the increase of *x* (*x*=1, 2, and 4 here) due to the shielding of increasingly loaded Pt on the surface.

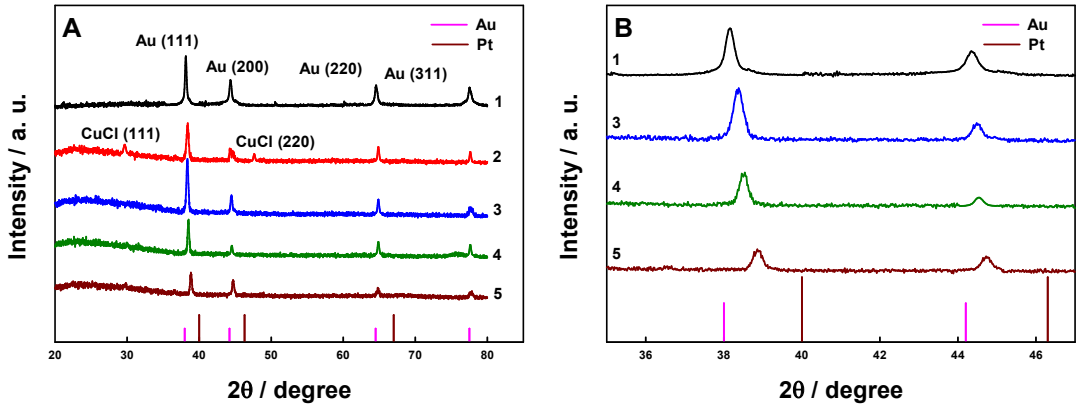

Fig. S9. (A) XRD patterns of QCM Au (1), CuCl/QCM Au (2), $Pt_{(CuCl)1}$/QCM Au (3), $Pt_{(CuCl)2}$/QCM Au (4) and $Pt_{(CuCl)4}$/QCM Au (5) and (B) the magnified images. The vertical lines at the bottom indicate the intensities of the corresponding reference polycrystalline samples (Au and Pt). Here, the observed four diffraction peaks at 38°, 44.2°, 64° and 77.5° on Au correspond well to the (111), (200), (220) and (311) crystal planes of *fcc* Au, respectively. The small peaks observed at 29.6° and 47.6° on CuCl/QCM Au can be attributed to crystal planes (111) and (220) of CuCl.[26] The XRD patterns of $Pt_{(CuCl)1}$/QCM Au, $Pt_{(CuCl)2}$/QCM Au and $Pt_{(CuCl)4}$/QCM Au are similar to those of Au, but the diffraction peaks of crystal planes (111) and (200) of Au are slightly positively shifted and the intensity is weakened with increasing the number of CuCl-electrodeposition/GRR cycles (B). No diffraction peak signal of Pt is observed in the above cases. A similar phenomenon can be found in a previous report,[9] implying that the Pt deposit here is very thin and hard to recognize clearly from XRD patterns.

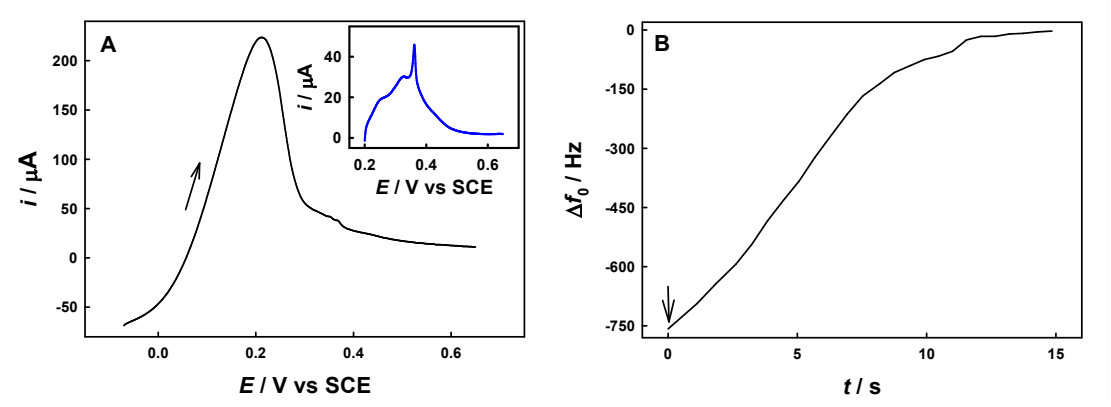

Fig. S10. LSASV curve (A) and corresponding time-dependent frequency response (B) of CuCl modified QCM Au electrodes that were obtained after potentiostating for 40 s at –0.07 V in 20 mM $CuSO_4$ + 100 mM HCl. Scan rate: 50 mV s^{-1}. Inset in panel A: an independent LSASV experiment on Cu_{UPD} modified QCM Au electrode that was obtained after potentiostating for 40 s at 0.2 V under the same conditions. The downward arrow in panel B indicates the moment of starting the positive potential sweep. According to Eq. 1, the mass of 40-s electrodeposited CuCl on QCM Au can be estimated as follows: $m = (Q/nF)\times M_{CuCl}$ = $(5.58\times10^{-4}$ C/9.6485×10^{4} C $mol^{-1})\times98.999$ g mol^{-1} = 573 ng (A), where the electrical charge of ca. 9.4×10^{-5} C for stripping of Cu UPD (Inset of panel A) is deducted here. Generally, the mass changes and the corresponding frequency changes (Δf_0) on QCM Au electrode should obey the Sauerbrey equation,[27-29] $\Delta f_0 = (-2.264\times10^{-6}\times f_{0g}^2\times\Delta m)/A$, where f_{0g} (9 MHz) is the fundamental frequency in air, and A (0.14 cm^2 here) is the geometric area of electrode. Thus, the mass of electrodeposited CuCl on QCM Au (Δf_0 = –700 Hz) is calculated to be $-700\times0.14/(-2.264\times10^{-6}\times(9\times10^{6})^2)$ = 532 ng (B). The Cu UPD effect is also deducted here (ca. –55 Hz based on Fig. S9). The CuCl mass obtained from QCM method and voltammetric analysis agree well with each other, proving the fidelity of our QCM. Hence, the number of CuCl monolayers is 532/52.4 = 10.2 (from QCM frequency response) and is 573/52.4 = 10.9 (from voltammetric response) on QCM Au ($S_{r\text{-}Au}$ = 0.4 cm^2, experimentally measured by following procedures similar to those at disk Au/GCE) based on Scheme S1. The results on QCM electrode agree acceptably with that on Au/GCE (8.84 CuCl layers). Note the varied

experimental conditions here, i.e., stopping of cathodic potential soon after the 40-s CuCl electrodeposition, immediate water-rinse of the electrode and then transfer to a separate 100 mM HCl solution for anodic stripping of CuCl on Au/GCE, versus in-situ anodic stripping of CuCl from −0.07 V (CuCl electrodeposition should continue for some additional time) on QCM Au.

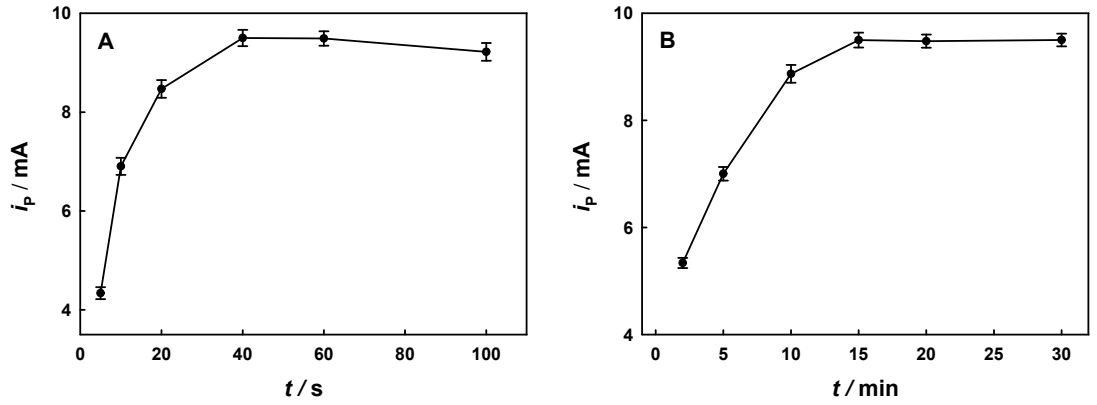

Fig. S11. Optimization of the CuCl-electrodeposition time (A) and the GRR time (B) from catalytic oxidation peak current by CV on $Pt_{(CuCl)1}$/Au/GCE in 0.5 M KOH + 1.0 M CH_3OH. The oxidation peak current of methanol is increased with the increase of CuCl-electrodeposition time at first, but a too thick CuCl film cannot well increase the catalysis performance probably due to more notable aggregation of Pt after GRR. The peak current is increased with the increase of GRR time and reaches at the response maximum after 15 min, indicating that the reaction between CuCl and K_2PtCl_4 has already been saturated.

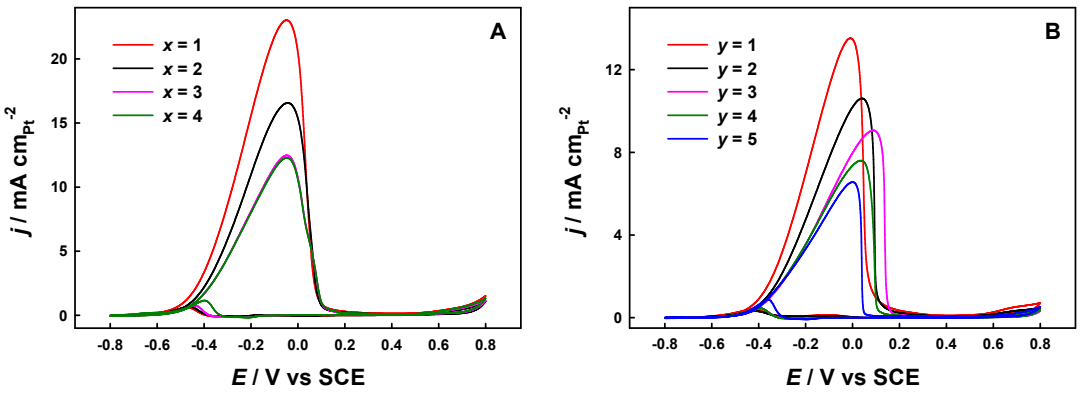

Fig. S12. CV curves of $Pt_{(CuCl)x}$/Au/GCEs (A) and $Pt_{(Cu\text{-}UPD)y}$/Au/GCEs (B) in 0.5 M KOH + 1.0 M CH_3OH. Currents are normalized to the $S_{r\text{-}Pt}$. Scan rate: 50 mV s^{-1}. Here, the $SECA_a$ for $Pt_{(CuCl)1}$/Au/GCE (23 mA cm_{Pt}^{-2}, at corresponding peak potentials of ca. −0.04 V) is ca. 1.7-fold that of $Pt_{(Cu\text{-}UPD)1}$/Au/GCE (13.4 mA cm_{Pt}^{-2}, at corresponding peak potentials of ca. 0 V). $Pt_{(CuCl)1}$/Au/GCE always gives a larger $SECA_a$ versus $Pt_{(Cu\text{-}UPD)y}$/Au/GCE when $x = y$, implying that the utilization of Pt by our method is very high.

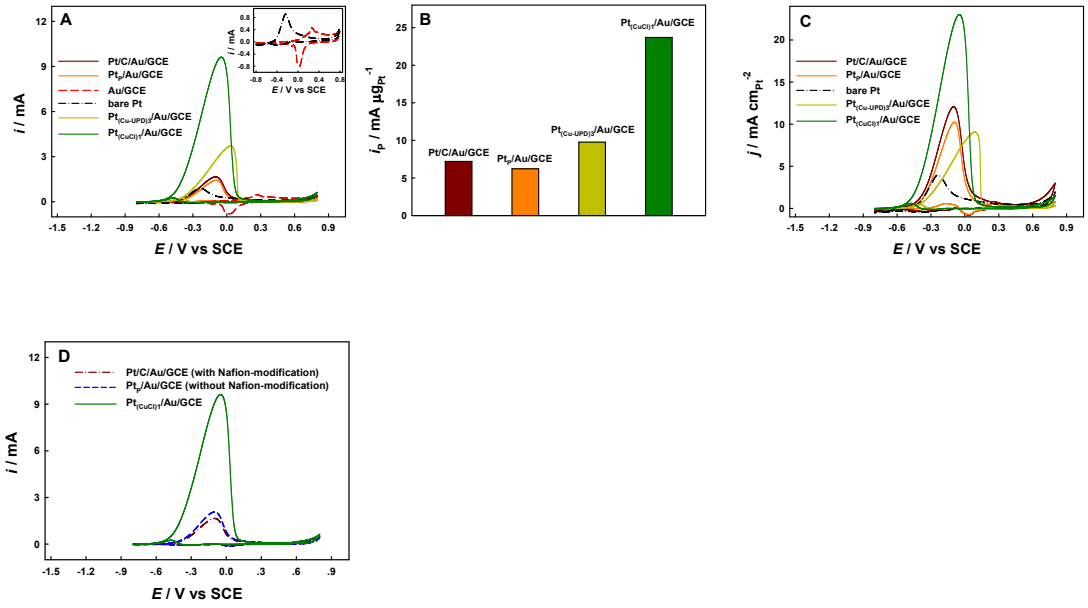

Fig. S13. CV curves of Pt/C/Au/GCE, Pt_p/Au/GCE, Au/GCE, bare Pt electrode, $Pt_{(Cu\text{-}UDP)3}$/Au/GCE and $Pt_{(CuCl)1}$/Au/GCE in 0.5 M KOH + 1.0 M CH_3OH (A), the corresponding $SECA_m$ (B) and $SECA_a$ (C). Inset: Enlarged plot for CV curves on Au/GCE and bare Pt electrode. Panel D shows the comparison of CV curves of Pt/C/Au/GCE (with Nafion-modification), Pt/C/Au/GCE (without Nafion-modification) and $Pt_{(CuCl)1}$/Au/GCE in 0.5 M KOH + 1.0 M CH_3OH. Scan rate: 50 mV s^{-1}. Here, the corresponding peak potentials are ca. −0.05 V ($Pt_{(CuCl)1}$/Au/GCE), ca. −0.09 V (Pt/C/Au/GCE), ca. −0.09 V (Pt_P/Au/GCE) and ca. 0.08 V ($Pt_{(Cu\text{-}UDP)3}$/Au/GCE) and ca. −0.23 V (bare Pt electrode). From panel D, we see that the peak current is ca. 25% larger than that of the Nafion-modified electrode. However, the catalytic performance of the Pt (20%)/C electrodes with and without Nafion modification is notably lower than that of the $Pt_{(CuCl)1}$/Au/GCE.

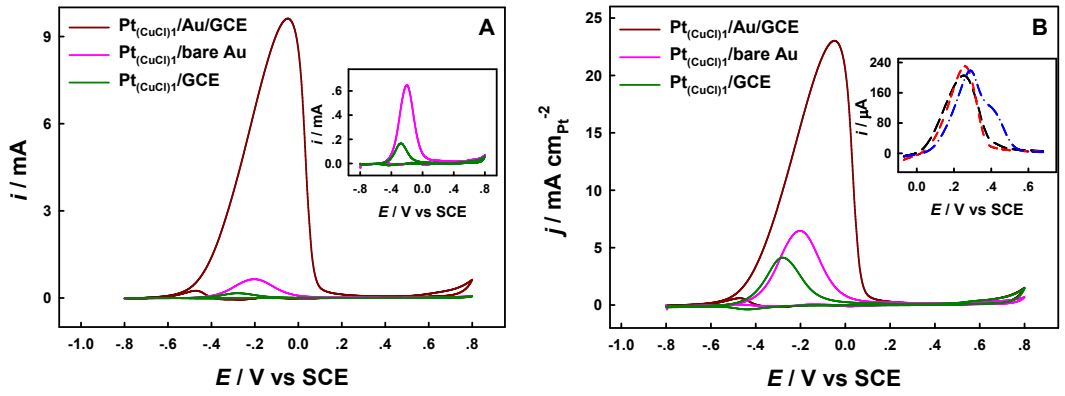

Fig. S14. CV curves of $Pt_{(CuCl)1}$/Au/GCE, $Pt_{(CuCl)1}$/bare Au and $Pt_{(CuCl)1}$/GCE in 0.5 M KOH + 1.0 M CH_3OH. Inset in panel A: Enlargement of CV curves of $Pt_{(CuCl)1}$/bare Au and $Pt_{(CuCl)1}$/GCE. Currents in panel B are normalized to $S_{r\text{-}Pt}$. Scan rate: 50 mV s^{-1}. Inset in panel B: LSASV curves at −0.07 V in 100 mM HCl on CuCl/Au/GCE, CuCl/bare Au and CuCl/GCE that were obtained after potentiostating at −0.07 V for 40 s on Au/GCE, for 60 s on bare Au and for 100 s on GCE in 20 mM $CuSO_4$ + 100 mM HCl, respectively, followed by immediate rinse with pure water. Here, the ultrathin Pt modified smooth GCE ($Pt_{(CuCl)1}$/GCE) and smooth bare Au electrode ($Pt_{(CuCl)1}$/bare Au) prepared by the CuCl-electrodeposition/GRR approach under similar experimental conditions (electrodepositing CuCl at −0.07 V and then one GRR cycle) were examined for electrocatalytic oxidation of methanol. For comparison, the electrical charges under the ASV peak of CuCl on bare Au (8.98×10^{-4} C, stripping of Cu UPD is also deducted) and GCE (1.02×10^{-3} C) are approximately equal to that on Au/GCE (9.13×10^{-4} C) by regulating the CuCl-electrodeposition time (Inset in panel B), which ensures almost the same quantity of CuCl for the subsequent GRR on the three electrodes. $Pt_{(CuCl)1}$/bare Au gives the larger CV response and specific electrocatalytic activity ($SECA_a$) than $Pt_{(CuCl)1}$/GCE, and our $Pt_{(CuCl)1}$/Au/GCE gives the largest CV response and $SECA_a$ among them, due probably to the synergic effect of GRR-induced Pt and Au substrate (especially electrodeposited Au substrate of some nano effects) for improved electrocatalytic oxidation of methanol.

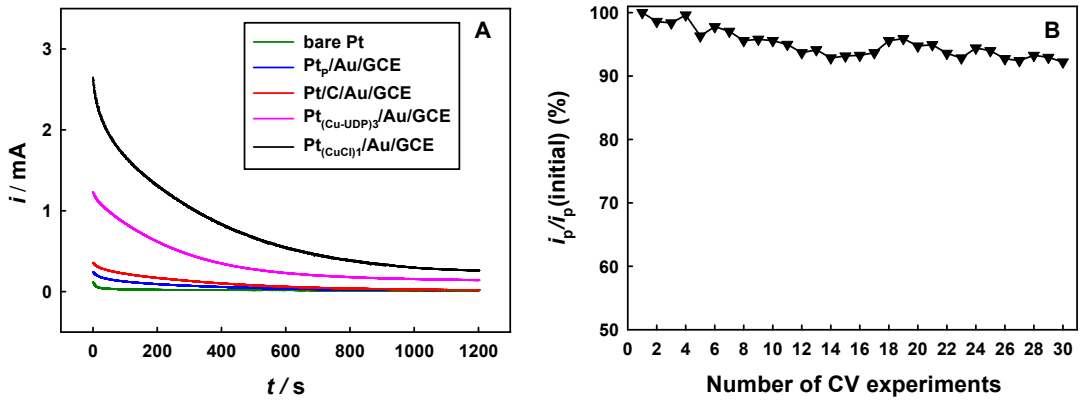

Fig. S15. (A) The *i-t* curves at −0.3 V on bare Pt, Pt/C/Au/GCE, Pt_P/Au/GCE, $Pt_{(Cu\text{-}UDP)3}$/Au/GCE and $Pt_{(CuCl)1}$/Au/GCE in 0.5 M KOH + 1.0 M CH_3OH under stirring conditions. (B) The stability of oxidation peak current (each for the first CV cycle) on $Pt_{(CuCl)1}$/Au/GCE during repeated CV experiments in 0.5 M KOH + 1.0 M CH_3OH. CV parameters: −0.8 V ~ 0.8 V, 50 mV s^{-1}, three cycles for each CV experiment. Here, the $Pt_{(CuCl)1}$/Au/GCE with a thicker Pt deposit is prepared by our method, and the thicker multilayer Pt electrocatalyst is more robust and less vulnerable during long-term catalysis applications.

References (The numbering here is only for the ESI)

1 L. Chao, W. Wang, M. Dai, Y. Ma, L. Sun, X. Qin, Q. Xie, *J. Electroanal. Chem.*, 2016, **778**, 66.

2 S. Trasatti, O. A. Petrii, *Pure Appl. Chem.*, 1991, **63**, 711.

3 L. J. Bu, T. A. Gu, Y. X. Ma, C. Chen, Y. M. Tan, Q. J. Xie, S. Z. Yao, *J. Phys. Chem. C*, 2015, **119**, 11400.

4 L. Han, S. Zhang, L. H. Han, D. P. Yang, C. T. Hou, A. Liu, *Electrochim. Acta*, 2014, **138**, 109.

5 T. Kondo, T. Masuda, N. Aoki, K. Uosaki, *J. Phys. Chem. C*, 2016, **120**, 16118.

6 B. Łosiewicz, R. Jurczakowski, A. Lasia, *Electrochim. Acta*, 2012, **80**, 292.

7 P. Liu, X. Ge, R. Wang, H. Ma, Y. Ding, *Langmuir* 2009, **25**, 561.

8 Z. Huang, Y. Liu, F. Xie, Y. Fu, Y. He, M. Ma, Q. Xie, S. Yao, *Chem. Commun.* , 2012, **48**, 12106.

9 P. Gnanaprakasam, S. E. Jeena, T. Selvaraju, *J.Mater.Chem.A* 2015, **3**, 18010.

10 I. A. Suleiman, M. W. Radny, M. J. Gladys, P. V. Smith, J. C. Mackie, E. M. Kennedy, B. Z. Dlugogorski, *Phys. Chem. Chem. Phys.*, 2015, **17**, 7038.

11 M. Mantina, A. C. Chamberlin, R. Valero, C. J. Cramer, D. G. Truhlar, *J. Phys. Chem. A*, 2009, **113**, 5806.

12 T. K. Ghanty, S. K. Ghosh, *J. Phys. Chem.*, 1994, **98**, 9197.

13 A. Bondi, *J. Phys. Chem.*, 1964, **68**, 441.

14 G. Zhang, Z. Yang, W. Zhang, Y. Wang, *J. Mater. Chem. A*, 2016, **4**, 3316.

15 W. Hong, J. Wang, E. Wang, *Small*, 2014, **10**, 3262.

16 Y. Lou, C. Li, X. Gao, T. Bai, C. Chen, H. Huang, C. Liang, Z. Shi, S. Feng, *ACS Appl. Mater. Interfaces*, 2016, **25**, 16147.

17 W. Zhang, J. Yang, X. Lu, *ACS Nano*, 2012, **6**, 7397.

18 K. L. Nagashree, M. F. Ahmed, *Synthetic Met.*, 2008, **158**, 610.

19 W. Huang, H. Wang, J. Zhou, J. Wang, P. N. Duchesne, D. Muir, P. Zhang, N. Han, F. Zhao, M. Zeng, J. Zhong, C. Jin, Y. Li, S. T. Lee, H. Dai, *Nat. Commun.*, 2015, **6**, 10035.

20 S. Ghosh, S. Bera, S. Bysakhb, R. N. Basu, *Sustainable Energy & Fuels*, 2017, **1**, 1148.

21 S. Emin, F. F. Abdi, M. Fanetti, W. Peng, W. Smith, K. Sivula, B. Dam, M. Valant, *J. Electroanal. Chem.*, 2014, **717-718**, 243.

22 D. M. Soares, S. Wasle, K. G. Weil, K. Doblhofer, *J. Electroanal. Chem.* , 2002, **532**, 353.

23 H. Tang, J. H. Chen, M. Y. Wang, L. H. Nie, Y. F. Kuang, S. Z. Yao, *Appl. Catal. A-Gen.*, 2004, **275**, 43.

24 J. J. Fritz, *J. Chem. Eng. Data*, 1982, **27**, 188.

25 R. Wang, J. Liu, P. Liu, X. Bi, X. Yan, W. Wang, X. Ge, M. Chen, Y. Ding, *Chem. Sci.*, 2014, **5**, 403.

26 Y. T. Lin, J. W. Ci, W. C. Tu, W. Y. Uen, S. M. Lan, T. N. Yang, C. C. Shen, C. H. Wu, *Thin Solid Films*, 2015, **591**, 43.

27 S. G., *Z. Phys.*, 1959, **155**, 206.

28 Q. Xie, JinWang, A. Zhou, Y. y. Zhang, H. Liu, Z. Xu, Y. Yuan, M. Deng, S. Yao, *Anal. Chem.*, 1999, **71**, 4649.

29 Q. Xie, Z. Li, C. Deng, M. Liu, Y. Zhang, M. Ma, S. Xia, X. Xiao, D. Yin, S. Yao, *J. Chem. Educ.*, 2007, **84**, 681.